Mechanics Research Communications 108 (2020) 103570

Contents lists available at ScienceDirect

Mechanics Research Communications

journal homepage: www.elsevier.com/locate/mechrescom

Variational multiscale modeling of Langmuir turbulent boundary layers in shallow water using Isogeometric Analysis

Qiming Zhu[a], Jinhui Yan[a], Andrés E. Tejada-Martínez[b], Yuri Bazilevs[c,*]

[a] Department of Civil and Environmental Engineering, University of Illinois Urbana-Champaign, United States
[b] Department of Civil and Environmental Engineering, University of South Florida, United States
[c] School of Engineering, Brown University, United States

ARTICLE INFO

Article history:
Received 12 March 2020
Revised 8 May 2020
Accepted 19 May 2020
Available online 29 July 2020

Keywords:
Langmuir turbulence
LES
IGA
RBVMS

ABSTRACT

We present large-eddy simulations (LES) of wind and wave-driven turbulent boundary layers in shallow water with Langmuir circulation using a variational multi-scale formulation of the Craik-Leibovich equations. The simulations are performed using Isogeometric Analysis (IGA) based on quadratic non-uniform rational basis spline (NURBS) basis functions. Wind and wave-driven turbulent boundary layers over a flat bottom surface representative of open ocean conditions in inner-shelf regions with turbulent Langmuir number $La_t = 0.7$ and wind stress friction Reynolds number $Re_\tau = 395$ are first simulated. The present results agree well with the reference results based on a spectral LES with higher mesh resolution [1]. Then, to investigate the effect of seabed topography on the turbulence, we simulate turbulent boundary layers over a sloped bottom surface with wind and wave forcing parallel to the shore, representative of a surf-shelf transition zone. We find that the Langmuir cell size increases as the water column shallows approaching onshore and the cell center shifts to the onshore direction. The mean velocity and turbulent kinetic energy along the shore are quantified.

1. Introduction

Langmuir turbulence is an environmental flow phenomenon with Langmuir circulation (LC) structures that consists of pairs of parallel counter-rotating cells (vortices) roughly aligned in the wind direction [1–3]. Langmuir turbulence is widely observed in the ocean and has been a long-standing fundamental problem in geophysics. Langmuir turbulence can be modeled by the Craik–Leibovich equations (C– L equations) [4], which are based on the Navier–Stokes equations of incompressible flows augmented with a vortex force term (known as Craik–Leibovich force or C-L force) in the momentum equations. The C–L vortex force, defined as the cross product between the Stokes drift velocity and the fluid vorticity, represents the interaction between the Stokes drift induced by surface gravity waves and vertical shear of the wind-driven current. Direct numerical simulations of the Craik-Leibovich equations require massive computational resources due to the interaction between the surface waves and the shear currents across a wide range of spatial and temporal scales. To effectively investigate higher Reynolds number Langmuir turbulence, large-eddy simulations (LES) are typically adopted. In this paper, departing from traditional LES models based on spectral methods or finite difference methods, we utilize a residual-based variational multiscale (RBVMS) [5] turbulence model to solve the C–L equations. We discretize the formulation using isogeometric analysis (IGA) [6,7] based on quadratic non-uniform rational basis spline (NURBS) elements. Research [8–19] has proven RBVMS and its moving-domain version [20–28] as effective methods to model high Reynolds number turbulent flows (both single-phase and multi-phase) in many fundamental and industrial applications. The combination of RBVMS and IGA [5,11,29–32] can produces equivalent accuracy as traditional LES on intermediate meshes and converge to DNS results. This is attributed to the higher accuracy per-degree-of-freedom of the IGA basis and the variational consistency of the RBMVS. In this paper, the IGA-based RBVMS is utilized to quantify the LC structures and important turbulence statistics of Langmuir boundary layers relevant to ocean science. We first simulate the case with a flat bottom surface and compare the results with spectral LES results with higher mesh resolution [1]. Then, the Langmuir boundary layers with a sloped bottom surface are further simulated to investigate the effect of seabed topography on the flow structures.

* Corresponding author.
E-mail address: yuri_bazilevs@browm.edu (Y. Bazilevs).

https://doi.org/10.1016/j.mechrescom.2020.103570
0093-6413/

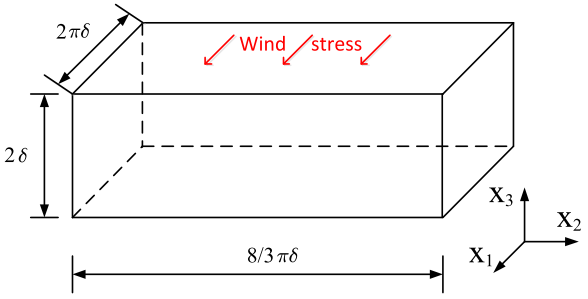

Fig. 1. Problem setup of the flat bottom surface case.

We present the paper as follows. Section 2 presents the governing equations of Langmuir turbulence and the corresponding RBVMS formulation. Section 3 presents the simulations of Langmuir turbulent boundary layers with a flat bottom surface and a sloped bottom surface. Conclusions are drawn in Section 4.

2. Numerical method

2.1. Craik-Leibovich equations

Langmuir turbulent boundary layers are governed by the Craik–Leibovich equations, which are based on Navier–Stokes equations of incompressible flows augmented with the C–L force term in the momentum equations, given as:

$$\mathbf{r}_M(\mathbf{u},p) := \frac{\partial \mathbf{u}}{\partial t} + \nabla\cdot(\mathbf{u}\otimes\mathbf{u}) + \nabla p - \nabla\cdot(2\nu\nabla^s\mathbf{u}) - \mathbf{f} - \boldsymbol{\phi}\times\nabla\times\mathbf{u} = \mathbf{0} \tag{1}$$

$$r_c(\mathbf{u}) := \nabla\cdot\mathbf{u} = 0 \tag{2}$$

where $\mathbf{u} = (u_1, u_2, u_3)^T$ is the velocity vector, p is the pressure, ν is the kinematic viscosity, $\nabla = (\partial/\partial x_1, \partial/\partial x_2, \partial/\partial x_3)^T$ is the gradient operator, ∇^s is the symmetric part of the gradient operator, $\mathbf{f}$ is the body force per unit mass, $\boldsymbol{\phi} = (\phi_1, \phi_2, \phi_3)^T$ is the depth-dependent Stokes drift velocity vector, induced by surface gravity waves. The definition of $\boldsymbol{\phi}$ will be specified next. The cross product between $\boldsymbol{\phi}$ and the flow vorticity $\nabla\times\mathbf{u}$ represents the C–L vortex force.

2.2. Residual-based variational multiscale formulation

We employ the residual-based variational multiscale formulation (RBVMS) [5,10] to solve the above governing equations. The semi-discrete formulation is stated as following. Let $\mathcal{V}_u$ and $\mathcal{V}_p$ denote the discrete velocity and pressure trial function spaces, and $\mathcal{W}_u$ and $\mathcal{W}_p$ denote the corresponding test function spaces. The RBVMS formulation of Langmuir turbulent boundary layers is stated as following. Find $\mathbf{u}^h \in \mathcal{V}_u$ and $p^h \in \mathcal{V}_p$, such that for all $\mathbf{w}^h \in \mathcal{W}_u$ and $q^h \in \mathcal{W}_p$,

$$B\big(\{\mathbf{w}^h, q^h\}, \{\mathbf{u}^h, p^h\}\big) + B_{\text{VMS}}\big(\{\mathbf{w}^h, q^h\}, \{\mathbf{u}^h, p^h\}\big) - F\big(\{\mathbf{w}^h, q^h\}\big) = 0 \tag{3}$$

where B and B_{VMS} are the Galerkin formulation and fine-scale terms arising from RBVMS, respectively. B, B_{VMS}, and F are defined as

$$\begin{aligned} &B(\{\mathbf{w},q\},\{\mathbf{u},p\}) = \\ &\int_\Omega \mathbf{w}\cdot\frac{\partial\mathbf{u}}{\partial t}\,d\Omega - \int_\Omega \nabla^s\mathbf{w} : (\mathbf{u}\otimes\mathbf{u})\,d\Omega \\ &- \int_\Omega \nabla\cdot\mathbf{w}p\,d\Omega + \int_\Omega q\nabla\cdot\mathbf{u}\,d\Omega \\ &+ \int_\Omega \mathbf{w}\cdot\tilde{\mathbf{A}}_i\frac{\partial\mathbf{u}}{\partial x_i}\,d\Omega + \int_\Omega \nabla^s\mathbf{w} : 2\nu\nabla^s\mathbf{u}\,d\Omega \end{aligned} \tag{4}$$

$$\begin{aligned} &B_{\text{VMS}}(\{\mathbf{w},q\},\{\mathbf{u},p\}) = \\ &-\int_\Omega \nabla^s\mathbf{w} : (\mathbf{u}'\otimes\mathbf{u} + \mathbf{u}\otimes\mathbf{u}' + \mathbf{u}'\otimes\mathbf{u}')\,d\Omega \\ &-\int_\Omega \nabla\cdot\mathbf{w}p'\,d\Omega - \int_\Omega q\nabla\cdot\mathbf{u}'\,d\Omega \\ &-\int_\Omega \tilde{\mathbf{A}}_i^T\frac{\partial\mathbf{w}}{\partial x_i}\cdot\mathbf{u}'\,d\Omega \end{aligned} \tag{5}$$

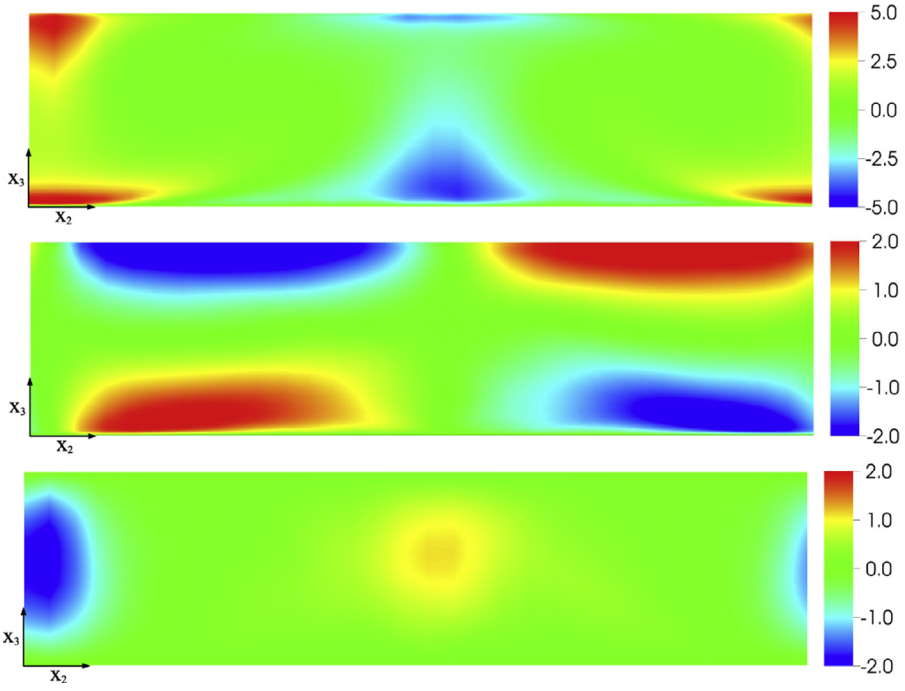

Fig. 2. Partially averaged fluctuation (u_i^p) for the flat bottom surface case. Top: streamwise direction (x_1 direction). Middle: crosswind direction (x_2 direction). Bottom: wall-normal direction (x_3 direction).

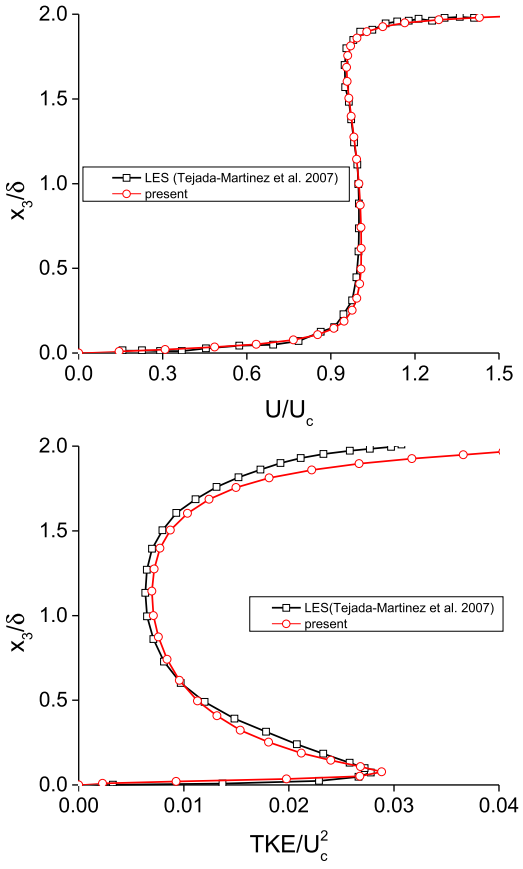

Fig. 3. Mean velocity (top) and TKE (bottom) in the wall-normal direction.

$$F(\{\mathbf{w}, q\}) = \int_{\Omega} \mathbf{w} \cdot \mathbf{f}\, d\Omega + \int_{\Gamma} \mathbf{w} \cdot \mathbf{h}\, d\Gamma \tag{6}$$

where $\mathbf{h}$ is the traction on the boundary Γ, which will incorporate the wind shear stress. (More details on the boundary conditions will be given in Section 3 along with the results for the cases considered.) Einstein summation is used for the repeated index. $\tilde{\mathbf{A}}_i$ $(i = 1, 2, 3)$ in Eq. (5) are the generalized advective matrices defined in terms of Stokes drift velocity components, namely,

$$\tilde{\mathbf{A}}_1 = \begin{bmatrix} 0 & -\phi_2 & -\phi_3 \\ 0 & \phi_1 & 0 \\ 0 & 0 & \phi_1 \end{bmatrix} \tag{7}$$

$$\tilde{\mathbf{A}}_2 = \begin{bmatrix} \phi_2 & 0 & 0 \\ -\phi_1 & 0 & -\phi_3 \\ 0 & 0 & \phi_2 \end{bmatrix} \tag{8}$$

$$\tilde{\mathbf{A}}_3 = \begin{bmatrix} \phi_3 & 0 & 0 \\ 0 & \phi_3 & 0 \\ -\phi_1 & -\phi_2 & 0 \end{bmatrix} \tag{9}$$

$\boldsymbol{u}'$ and p' in Eq. (5) are the fine-scale velocity and pressure. Analogously to [5], they are defined as

$$\mathbf{u}' = -\boldsymbol{\tau}_M \mathbf{r}_M(\mathbf{u}^h, p^h) \tag{10}$$

$$p' = -\tau_C \mathbf{r}_C(\mathbf{u}^h) \tag{11}$$

where $\boldsymbol{\tau}_M$ and τ_C are the SUPG [33] and PSPG [34,35] parameters. To define $\boldsymbol{\tau}_M$ for the C–L equations, we re-write the left hand side of the momentum equations as a quasi-linear advective-diffusive system, namely,

$$\mathbf{r}_M(\mathbf{u}, p) = \frac{\partial \mathbf{u}}{\partial t} + \mathbf{A}_i \cdot \frac{\partial \mathbf{u}}{\partial x_i} + \nabla p - \nabla \cdot (2\nu \nabla^s \mathbf{u}) - \mathbf{f} \tag{12}$$

where $\mathbf{A}_i = \tilde{\mathbf{A}}_i + u_i \mathbf{I}$ is the "effective" advective flux Jacobian. Following the developments in [36–38] for multi-dimensional advective-diffusive systems, $\boldsymbol{\tau}_M$ is computed as

$$\boldsymbol{\tau}_M = \left(\frac{4}{\Delta t^2} \mathbf{I} + \mathbf{A}_i G_{ij} \mathbf{A}_j + C_I G_{ij} G_{ij} \nu^2 \mathbf{I} \right)^{-\frac{1}{2}} \tag{13}$$

where Δt is the time step of the simulation, $\mathbf{G}$ is the mesh element metric tensor of the mapping from the parametric domain to the physical domain. C_I is a constant arising in the element-level inverse estimate [39]. The matrix square root inverse is done by the Denman–Beavers algorithm [40].

The above RBMVS formulation is integrated in time by the generalized-α method [41]. Newton–Raphson method is applied to linearize the equations. The resulting linear equation systems are solved using a generalized minimal residual method (GMRES) approach [42] with diagonal preconditioning.

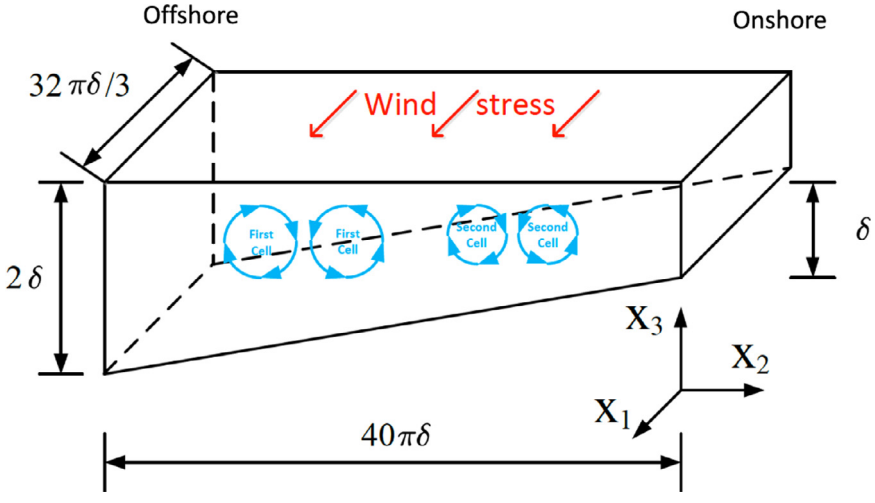

Fig. 4. Problem setup for the sloped bottom surface case.

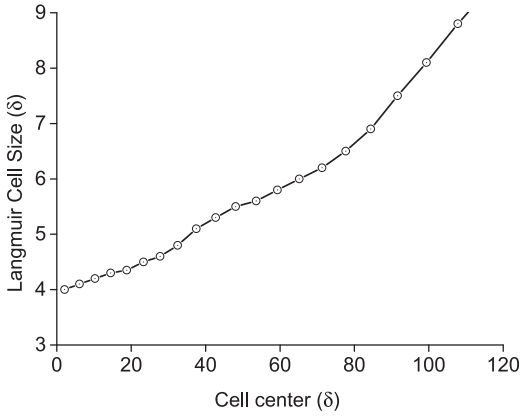

Fig. 5. Langmuir cell size along the shore (x_2).

3. Results

In this section, Langmuir turbulent boundary layers are simulated with both flat bottom surface and sloped bottom surface. The flow is driven by a wind shear $\mathbf{h} = (h, 0, 0)^T$. The body force $\mathbf{f} = 0$. The flow can be characterized by the turbulent Langmuir number $La_t = \sqrt{u_s/u_\tau}$ and friction Reynolds number $Re_\tau = u_\tau \delta/\nu$, where u_s is a characteristic Stokes drift velocity [1] and u_τ is the wind stress friction velocity.

3.1. Flat bottom surface

We first simulate Langmuir turbulence boundary layers with a flat bottom surface at $La_t = 0.7$ and $Re_\tau = 395$ following [1]. The Stokes drift velocity is chosen as $\boldsymbol{\phi} = (u_s \frac{\cosh(2\kappa x_3)}{2\sinh^2(2\kappa\delta)}, 0, 0)^T$, where κ is the dominant wave number. In present work, $\kappa = 12\delta$, u_s, and δ and ν are chosen such that the desired La_t and Re_τ are achieved.

Fig. 1 shows the problem setup. The computation domain is a box with dimensions $2\pi\delta \times \frac{8\pi\delta}{3} \times 2\delta$. The mesh consist of $32 \times 32 \times 34$ C^1-continuous quadratic NURBS elements. The elements in the wall-normal direction (x_3) are stretched towards the top surface ($x_3 = 2\delta$) and bottom surface ($x_3 = 0$) to better resolve the boundary layers. Periodic boundary condition is used in the stream-wise (x_1) and crosswind (x_2) directions, representative of open ocean conditions unaffected by lateral boundaries. No-penetration boundary condition is applied at the top surface in addition to wind shear stress. No-slip condition is applied at the bottom surface through the weak enforcement of essential boundary condition approach (weak BC). For weak BC, we refer the readers to [32,43] for the original development and [11,14,44–49] for several applications to CFD and fluid-structure interaction (FSI) problems.

To extract the crosswind-vertical (x_2–x_3 plane) flow structure, the following triple decomposition is adopted.

$$u_i = \langle u_i \rangle + u_i' = \langle u_i \rangle + \langle u_i' \rangle_{tx_1} + u_i'' \tag{14}$$

where $\langle \cdot \rangle$ without subscript denotes the averaging operation over time, the stream-wise and crosswind directions, $\langle \cdot \rangle_{tx_1}$ denotes the averaging operation over time and the stream-wise direction. So the partially averaged fluctuation is given by $u_i^p = \langle u_i' \rangle_{tx_1}$. (Note the subscript $'$ here denotes fluctuation in Reynolds averaging, and not the fine unresolved scales as in Eq. 5.)

Fig. 2 shows the partially averaged fluctuations of the velocity components in the stream-wise (x_1), crosswind (x_2), and wall-normal (x_3) directions, normalized by the friction velocity u_τ. These fluctuations reveal the resolution of a single Langmuir cell occupying the entire crosswind width of the domain. The Langmuir cell structure can be observed in terms of crosswind and wall-normal components. The surface divergence of the cell corresponds to the surface divergence of positive and negative crosswind velocity fluctuations. Furthermore, the surface divergence is positioned directly above the upwelling limb of the cell, characterized by positive wall-normal velocity fluctuations. These visualizations qualitatively agree with the spectral LES results in [1] and field observations in [50]. Fig. 3 shows the mean velocity and turbulent kinetic energy (TKE) normalized by averaged center-line velocity (U_c) along the wall direction (averaging is performed over time, stream-wise, and crosswind directions). This problem was also simulated using a spectral LES with a higher resolution in [1]. The results are also plotted in Fig. 3 for comparison. Excellent agreement is achieved for the mean flow, and a reasonably good agreement is achieved for the TKE for the mesh resolution employed here.

3.2. Sloped bottom surface

To investigate the effect of seabed topography, we simulate Langmuir turbulence boundary layers over a sloped bottom sur-

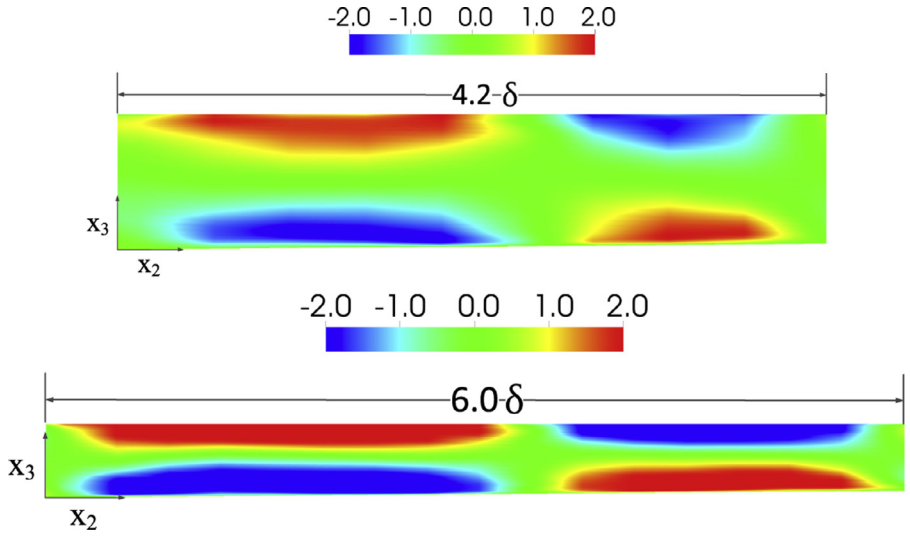

Fig. 6. Two representative Langmuir cells, visualized by partially averaged velocity fluctuations in crosswind direction (u_2^p). Top: offshore. Bottom: onshore.

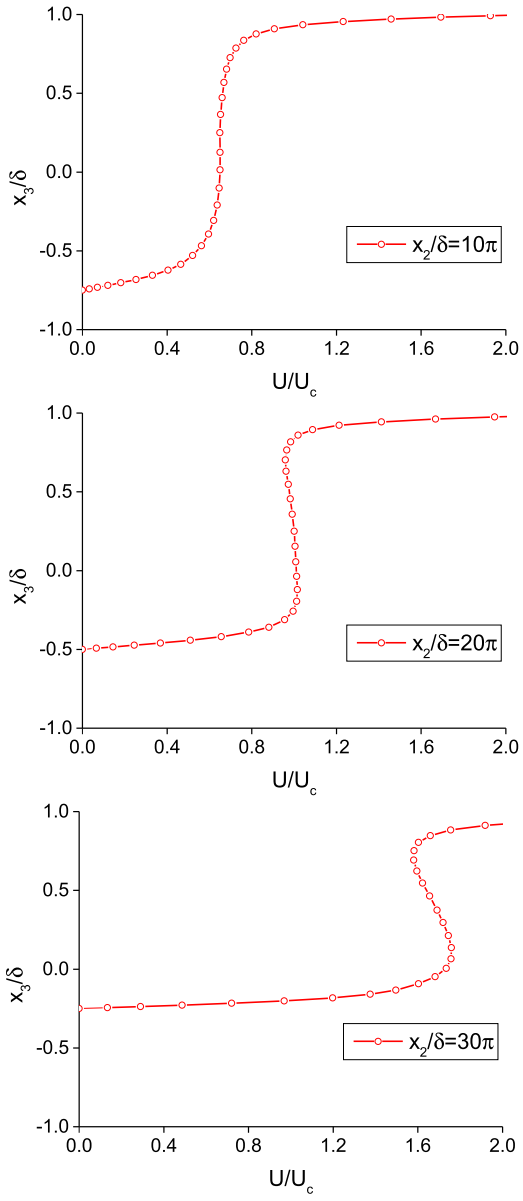

Fig. 7. Mean streamwise velocity for the sloped bottom surface.

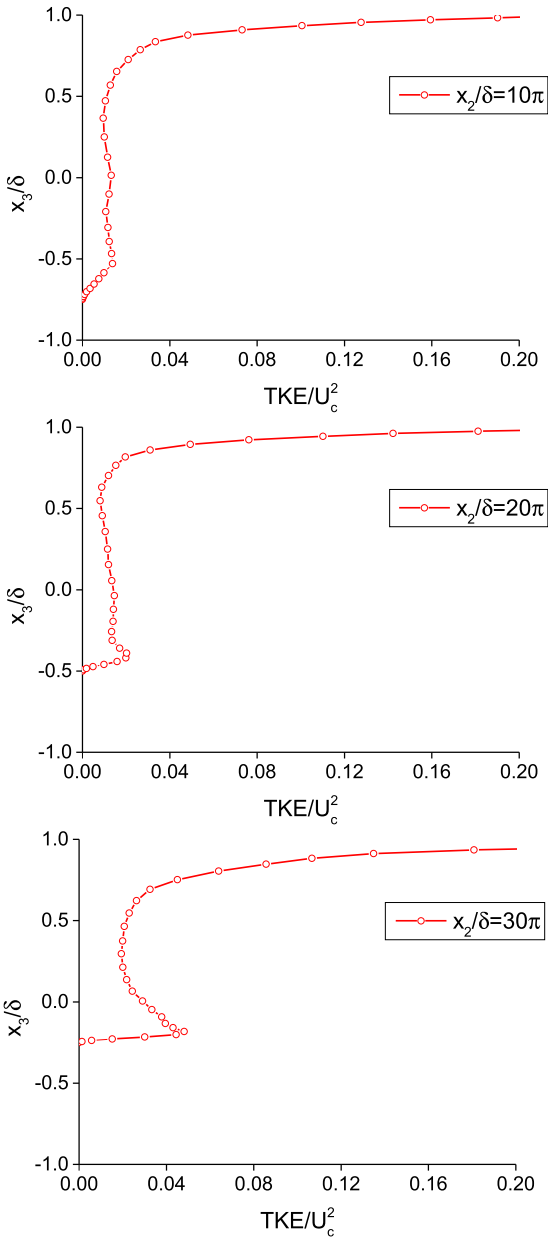

Fig. 8. TKE for the sloped bottom surface.

face. Fig. 4 shows the problem setup. The dimensions of the stream-wise and crosswind directions are $32\pi/3$ and 40π, respectively. The domain is significantly longer in the stream-wise and crosswind directions to allow resolution of multiple Langmuir cells. The water depth changes from 2δ to δ linearly from the offshore to the onshore. The mesh consists of $64 \times 144 \times 34$ C^1-continuous quadratic NURBS elements.

The boundary conditions are the same as in the previous section except no-penetration boundary condition is adopted for the crosswind direction. The wind stress is parallel to the shore. The mesh is also stretched towards the top and bottom surfaces to resolve the boundary layers better. Locally changing wind shear stress is applied on the top surface to achieve constant friction $Re_\tau = 395$ with respect to the local water depth. The Stokes drift velocity is defined as $\phi = (u_s \frac{\cosh(2\kappa x_3^l)}{2\sinh^2(2\kappa\delta^l)}, 0, 0)^T$, where δ^l is the local water half depth and x_3^l is the local distance to the bottom surface. Note that the waves (Stokes drift) are aligned with the wind.

The triple-decomposition in Eq. (14) is used again to extract the crosswind-vertical (x_2–x_3 plane) Langmuir cell structure. Fig. 5 shows the Langmuir cell size from offshore to onshore. The cell size increases approaching onshore. We present two representative Langmuir cells, one offshore and one onshore, in Fig. 6 by visualizing the partially averaged velocity fluctuations along the crosswind (x_2) direction. Fig. 6 also indicates that the center of the cells slightly shifts to the onshore direction. Since the crosswind direction is no longer periodic, we quantify the mean velocity and turbulent kinetic energy (TKE) by only averaging over time and the stream-wise direction. Fig. 7 and Fig. 8 show mean velocity and TKE along three lines ($x_2 = 10\pi\delta, 20\pi\delta,$ and $30\pi\delta$). The mean velocity and TKE are normalized by the local center velocity U_c^l at the current x_2 coordinate. It can be seen that the vertical mixing of momentum induced by the cells increases with decreasing distance to the shore. Furthermore, the near bottom TKE also increases with decreasing distance to the shore.

4. Conclusion

We simulated Langmuir turbulent boundary layers in shallow water using a residual-based variational multi-scale formulation (RBVMS) with quadratic NURBS basis functions. Simulations showed the combination of RBVMS and IGA can produce accurate results with a relatively coarse mesh. We quantified the turbulence statistics, including partially averaged velocity fluctuations, mean velocity, and TKE, of the Langmuir turbulent boundary layers over a sloped bottom surface. In an idealized setup with wind and waves parallel to the shore, we found that the Langmuir cell size increases with decreasing distance to the shore. For each cell, the cell center shifts slightly to the onshore direction. The simulations show the potential of the numerical methods for understanding Langmuir turbulence in coastal regions, which is a fundamental problem in coastal physical oceanography. In the future we hope to make use of these numerical simulations to investigate Langmuir turbulence under more realistic conditions by considering bottom roughness, misaligned wind and waves and higher Reynolds numbers.

Declaration of Competing Interest

The authors have no conflict of interest pertaining to the submitted manuscript.

Acknowledgment

Q. Zhu is partially supported by a seed grant from the Institute for Sustainability, Energy, and Environment (iSEE) at University of Illinois at Urbana-Champaign. Y. Bazilevs was supported through the National Science Foundation (NSF) Award No. 1854436. A. E. Tejada-Martínez was supported through the NSF Award No. 1806786. This support is gratefully acknowledged.

References

[1] A. Tejada-Martinez, C. Grosch, Langmuir turbulence in shallow water. Part 2. Large-eddy simulation, J. Fluid Mech. 576 (2007) 63–108.
[2] R. Golshan, A. Tejada-Martínez, M. Juha, Y. Bazilevs, Les and rans simulation of wind-and wave-forced oceanic turbulent boundary layers in shallow water with wall modeling, Comput. Fluids 142 (2017) 96–108.
[3] A. Gargett, J. Wells, A. Tejada-Martinez, C. Grosch, Langmuir supercells: a mechanism for sediment resuspension and transport in shallow seas, Science 306 (5703) (2004) 1925–1928.
[4] A. Craik, S. Leibovich, A rational model for Langmuir circulations, J. Fluid Mech. 73 (3) (1976) 401–426.
[5] Y. Bazilevs, V.M. Calo, J.A. Cottrell, T.J.R. Hughes, A. Reali, G. Scovazzi, Variational multiscale residual-based turbulence modeling for large eddy simulation of incompressible flows, Comput. Methods Appl. Mech. Eng. 197 (2007) 173–201.
[6] T.J.R. Hughes, J.A. Cottrell, Y. Bazilevs, Isogeometric analysis: CAD, finite elements, NURBS, exact geometry, and mesh refinement, Comput. Methods Appl. Mech. Eng. 194 (2005) 4135–4195.
[7] J.A. Cottrell, T.J.R. Hughes, Y. Bazilevs, Isogeometric Analysis. Toward Integration of CAD and FEA, Wiley, 2009.
[8] A. Masud, R. Calderer, A variational multiscale stabilized formulation for the incompressible Navier–Stokes equations, Comput. Mech. 44 (2) (2009) 145–160.
[9] S. Xu, N. Liu, J. Yan, Residual-based variational multi-scale modeling for particle-laden gravity currents over flat and triangular wavy terrains, Comput. Fluids 188 (2019) 114–124.
[10] A. Tejada-Martĩnez, I. Akkerman, Y. Bazilevs, Large-eddy simulation of shallow water Langmuir turbulence using isogeometric analysis and the residual-based variational multiscale method, J. Appl. Mech. 79 (1) (2012) 010909.
[11] J. Yan, A. Korobenko, A. Tejada-Martínez, R. Golshan, Y. Bazilevs, A new variational multiscale formulation for stratified incompressible turbulent flows, Comput. Fluids 158 (2017) 150–156.
[12] T.M. van Opstal, J. Yan, C. Coley, J.A. Evans, T. Kvamsdal, Y. Bazilevs, Isogeometric divergence-conforming variational multiscale formulation of incompressible turbulent flows, Comput. Methods Appl. Mech. Eng. 316 (2017) 859–879.
[13] M. ten Eikelder, Y. Bazilevs, I. Akkerman, A theoretical framework for discontinuity capturing: joining variational multiscale analysis and variation entropy theory, Comput. Methods Appl. Mech. Eng. 359 (2020) 112664.
[14] J. Yan, A. Korobenko, X. Deng, Y. Bazilevs, Computational free-surface fluid–structure interaction with application to floating offshore wind turbines, Comput. Fluids 141 (2016) 155–174.
[15] J. Yan, X. Deng, A. Korobenko, Y. Bazilevs, Free-surface flow modeling and simulation of horizontal-axis tidal-stream turbines, Comput. Fluids 158 (2017) 157–166.
[16] J. Yan, W. Yan, S. Lin, G.J. Wagner, A fully coupled finite element formulation for liquid–solid–gas thermo-fluid flow with melting and solidification, Comput. Methods Appl. Mech. Eng. 336 (2018) 444–470.
[17] A. Masud, R. Calderer, A variational multiscale method for incompressible turbulent flows: bubble functions and fine scale fields, Comput. Methods Appl. Mech. Eng. 200 (33–36) (2011) 2577–2593.
[18] Y. Bazilevs, K. Kamran, G. Moutsanidis, D. Benson, E. Oñate, A new formulation for air-blast fluid–structure interaction using an immersed approach. Part I: Basic methodology and fem-based simulations, Comput. Mech. 60 (1) (2017) 83–100.
[19] Y. Bazilevs, G. Moutsanidis, J. Bueno, K. Kamran, D. Kamensky, M. Hillman, H. Gomez, J. Chen, A new formulation for air-blast fluid–structure interaction using an immersed approach: Part II-Coupling of IGA and meshfree discretizations, Comput. Mech. 60 (1) (2017) 101–116.
[20] Y. Bazilevs, V.M. Calo, T.J.R. Hughes, Y. Zhang, Isogeometric fluid–structure interaction: theory, algorithms, and computations, Comput. Mech. 43 (2008) 3–37.
[21] K. Takizawa, Y. Bazilevs, T.E. Tezduyar, Space–time and ALE-VMS techniques for patient-specific cardiovascular fluid–structure interaction modeling, Arch. Comput. Methods Eng. 19 (2012) 171–225, doi:10.1007/s11831-012-9071-3.
[22] J. Yan, X. Deng, F. Xu, S. Xu, Q. Zhu, Numerical simulations of two back-to-back horizontal axis tidal stream turbines in free-surface flows, J. Appl. Mech. 87 (6) (2020).
[23] K. Takizawa, D. Montes, S. McIntyre, T.E. Tezduyar, Space–time VMS methods for modeling of incompressible flows at high Reynolds numbers, Math. Models Methods Appl. Sci. 23 (2013) 223–248, doi:10.1142/s0218202513400022.
[24] Y. Bazilevs, M.-C. Hsu, K. Takizawa, T.E. Tezduyar, ALE-VMS and ST-VMS methods for computer modeling of wind-turbine rotor aerodynamics and fluid–structure interaction, Math. Models Methods Appl. Sci. 22 (supp02) (2012) 1230002, doi:10.1142/S0218202512300025.
[25] Y. Bazilevs, K. Takizawa, T.E. Tezduyar, Computational Fluid-Structure Interaction: Methods and Applications, Wiley, 2013.
[26] T.E. Tezduyar, K. Takizawa, Y. Bazilevs, Fluid–structure interaction and flows with moving boundaries and interfaces, in: Encyclopedia of Computational Mechanics Second Edition, 2018, pp. 1–53.
[27] J. Liu, A. Oberai, The residual-based variational multiscale formulation for the large eddy simulation of compressible flows, Comput. Methods Appl. Mech. Eng. 245 (2012) 176–193.
[28] D. Sondak, J. Shadid, A. Oberai, R. Pawlowski, E. Cyr, T. Smith, A new class of finite element variational multiscale turbulence models for incompressible magnetohydrodynamics, J. Comput. Phys. 295 (2015) 596–616.
[29] Y. Bazilevs, T.J.R. Hughes, NURBS-based isogeometric analysis for the computation of flows about rotating components, Comput. Mech. 43 (2008) 143–150.
[30] Y. Bazilevs, I. Akkerman, Large eddy simulation of turbulent Taylor–Couette flow using isogeometric analysis and the residual–based variational multiscale method, J. Comput. Phys. 229 (2010) 3402–3414.
[31] J. Yan, S. Lin, Y. Bazilevs, G. Wagner, Isogeometric analysis of multi-phase flows with surface tension and with application to dynamics of rising bubbles, Comput. Fluids 179 (2019) 777–789.
[32] Y. Bazilevs, C. Michler, V.M. Calo, T.J.R. Hughes, Isogeometric variational multiscale modeling of wall-bounded turbulent flows with weakly enforced boundary conditions on unstretched meshes, Comput. Methods Appl. Mech. Eng. 199 (2010) 780–790.
[33] A.N. Brooks, T.J.R. Hughes, Streamline upwind/Petrov-Galerkin formulations for convection dominated flows with particular emphasis on the incompressible Navier-Stokes equations, Comput. Methods Appl. Mech. Eng. 32 (1982) 199–259.
[34] T.E. Tezduyar, Stabilization parameters and element length scales in SUPG and PSPG formulations, in: Book of Abstracts of An Euro Conference on Numerical Methods and Computational Mechanics, 2002 Miskolc, Hungary.
[35] T. Tezduyar, S. Sathe, Stabilization parameters in SUPG and PSPG formulations, J. Comput. Appl. Mech. 4 (2003) 71–88.
[36] F. Shakib, T.J.R. Hughes, Z. Johan, A multi-element group preconditionined GMRES algorithm for nonsymmetric systems arising in finite element analysis, Comput. Methods Appl. Mech. Eng. 75 (1989) 415–456.
[37] T.J.R. Hughes, M. Mallet, A new finite element formulation for computational fluid dynamics: III. The generalized streamline operator for multidimensional advective-diffusive systems, Comput. Methods Appl. Mech. Eng. 58 (1986) 305–328.
[38] T.J.R. Hughes, G. Scovazzi, T.E. Tezduyar, Stabilized methods for compressible flows, Journal of Scientific Computing 43 (2010) 343–368, doi:10.1007/s10915-008-9233-5. DOI: 10.1007/s10915-008-9233-5
[39] C. Johnson, Numerical Solution of Partial Differential Equations by the Finite Element Method, Cambridge University Press, Sweden, 1987.
[40] E. Denman, A. Beavers, The matrix sign function and computations in systems, Appl. Math. Comput. 2 (1) (1976) 63–94.
[41] K.E. Jansen, C.H. Whiting, G.M. Hulbert, A generalized-α method for integrating the filtered Navier–Stokes equations with a stabilized finite element method, Comput. Methods Appl. Mech. Eng. 190 (3–4) (2000) 305–319.

[42] Y. Saad, M. Schultz, GMRES: a generalized minimal residual algorithm for solving nonsymmetric linear systems, SIAM J. Sci. Stat. Comput. 7 (1986) 856–869.
[43] Y. Bazilevs, T.J.R. Hughes, Weak imposition of Dirichlet boundary conditions in fluid mechanics, Comput. Fluids 36 (2007) 12–26.
[44] R. Golshan, A. Tejada-Martínez, M. Juha, Y. Bazilevs, Large-eddy simulation with near-wall modeling using weakly enforced no-slip boundary conditions, Comput. Fluids 118 (2015) 172–181.
[45] Q. Zhu, F. Xu, S. Xu, M. Hsu, J. Yan, An immersogeometric formulation for free–surface flows with application to marine engineering problems, Comput. Methods Appl. Mech. Eng. 361 (2020) 112748.
[46] Q. Zhu, J. Yan, A moving-domain cfd solver in fenics with applications to tidal turbine simulations in turbulent flows, Comput. Math. Appl. (2019).
[47] M. Hsu, I. Akkerman, Y. Bazilevs, Wind turbine aerodynamics using ALE–VMS: validation and the role of weakly enforced boundary conditions, Comput. Mech. 50 (4) (2012) 499–511.
[48] B. Augier, J. Yan, A. Korobenko, J. Czarnowski, G. Ketterman, Y. Bazilevs, Experimental and numerical FSI study of compliant hydrofoils, Comput. Mech. 55 (2015) 1079–1090, doi:10.1007/s00466-014-1090-5.
[49] J. Yan, B. Augier, A. Korobenko, J. Czarnowski, G. Ketterman, Y. Bazilevs, FSI modeling of a propulsion system based on compliant hydrofoils in a tandem configuration, Comput. Fluids 141 (2016) 201–211.
[50] A. Gargett, J. Wells, Langmuir turbulence in shallow water. Part 1. Observations, J. Fluid Mech. 576 (2007) 27–61.